Published in final edited form as:
Ann Neurol. 2014 April ; 75(4): 581–590. doi:10.1002/ana.24128.

KCNT1 gain-of-function in two epilepsy phenotypes is reversed by quinidine

Carol J. Milligan, PhD[1,12], **Melody Li, BSc(Hons)**[1,12], **Elena V. Gazina, PhD**[1], **Sarah E. Heron, PhD**[2,3], **Umesh Nair, BSc(Hons)**[1], **Chantel Trager, BSc**[1], **Christopher A. Reid, PhD**[1], **Anu Venkat, MD**[4,5], **Donald P. Younkin, MD**[5], **Dennis J. Dlugos, MD**[4,5], **Slavé Petrovski, PhD**[6,7], **David B. Goldstein, PhD**[6], **Leanne M. Dibbens, PhD**[2,3], **Ingrid E. Scheffer, MBBS, PhD**[1,8,9], **Samuel F Berkovic, MD**[8], and **Steven Petrou, PhD**[1,10,11]

[1]Ion Channels & Disease Group, Epilepsy Division, The Florey Institute of Neuroscience and Mental Health, Parkville, Victoria, Australia.

[2]School of Pharmacy and Medical Sciences, University of South Australia, Adelaide, Australia.

[3]Sansom Institute for Health Research, University of South Australia, Adelaide, Australia.

[4]Perelman School of Medicine, University of Pennsylvania, Philadelphia, PA, USA.

[5]Departments of Pediatrics and Neurology, The Children's Hospital of Philadelphia, Philadelphia, PA, USA.

[6]Center for Human Genome Variation, Duke University School of Medicine, Durham, North Carolina, USA.

[7]Department of Medicine, Austin Health and Royal Melbourne Hospital, University of Melbourne, Austin Hospital, Heidelberg, Victoria, Australia.

[8]Epilepsy Research Centre, Department of Medicine, The University of Melbourne, Melbourne, Victoria, Australia.

[9]Department of Paediatrics, The University of Melbourne, Royal Children's Hospital, Melbourne, Victoria, Australia.

[10]Department of Anatomy and Neuroscience, The University of Melbourne, Melbourne, Victoria, Australia.

[11]Centre for Neural Engineering, The University of Melbourne, Melbourne, Victoria, Australia.

Corresponding author: A/Prof Steven Petrou, Florey Institute of Neuroscience and Mental Health, Kenneth Myer Building, 30 Royal Parade, Parkville, Victoria, Australia, 3010, 9035 3628, spetrou@unimelb.edu.au.

[12]These authors contributed equally to this work.

Authorship

C.J.M. designed the experiments, analyzed data and prepared the manuscript. M.L. designed and performed functional experiments. E.G. preformed qPCR experiments and analysis. S.E.H. performed genomics analysis. U.N. performed functional experiments. C.T. performed functional experiments. C.A.R. manuscript editing and contribution to experimental design. A.V. provided clinical information. D.P.Y. provided clinical information. D.J.D. provided clinical information. Slave. P. bioinformatics. D.B.G. bioinformatics and prepared the manuscript. L.M.D. performed genomics analysis. I.E.S. identified families and provided clinical information, manuscript editing. S.F.B. identified families and provided clinical information, manuscript editing. S.P. designed the experiments and prepared the manuscript.

Potential Conflicts of Interest

The authors declare no potential conflicts of interest.

Abstract

Objective—Mutations in *KCNT1* have been implicated in autosomal dominant nocturnal frontal lobe epilepsy (ADNFLE) and epilepsy of infancy with migrating focal seizures (EIMFS). More recently, a whole exome sequencing study of epileptic encephalopathies identified an additional *de novo* mutation in one proband with EIMFS. We aim to investigate the electrophysiological and pharmacological characteristics of h*KCNT1* mutations and examine developmental expression levels.

Methods—Here we use a *Xenopus laevis* oocyte based automated two-electrode voltage-clamp assay. The effects of quinidine (100 and 300 μM) are also tested. Using quantitative RT-PCR, the relative levels of mouse brain m*Kcnt1* mRNA expression are determined.

Results—We demonstrate that *KCNT1* mutations implicated in epilepsy cause a marked increase in function. Importantly, there was a significant group difference in gain-of-function between mutations associated with ADNFLE and EIMFS. Finally, exposure to quinidine significantly reduces this gain-of-function for all mutations studied.

Interpretation—These results establish direction for a targeted therapy and potentially exemplify a translational paradigm for *in vitro* studies informing novel therapies in a neuropsychiatric disease.

Introduction

Autosomal dominant nocturnal frontal lobe epilepsy (ADNFLE) is characterized by nocturnal frontal lobe seizures beginning in mid-childhood, with psychiatric, behavioural and cognitive disabilities in some cases[1]. In contrast, epilepsy of infancy with migrating focal seizures (EIMFS), previously known as malignant migrating partial seizures of infancy, is a severe early-onset epileptic encephalopathy beginning before the age of 6 months. It is characterized by heterogeneous focal seizures, where seizures appear to migrate from one brain region and hemisphere to another, and is associated with arrest or regression of development resulting in profound disability[2,3].

In addition to mutations in several neuronal nicotinic acetylcholine receptor subunits, the group of genes first identified in ADNFLE[4], a number of *KCNT1* mutations have been recently implicated in severe cases of ADNFLE including M896I, R398Q, Y796H and R928C[5]. Furthermore, V271F, G288S, R428Q, R474Q, I760M and A934T have been identified in patients with EIMFS[6–8]. More recently, an additional *de novo* mutation in *KCNT1* (P924L) was found in a patient with EIMFS in whom infantile spasms was part of the clinical evolution[9].

KCNT1 encodes a weakly voltage dependent and intracellular sodium activated potassium channel. *KCNT1* is a member of the *Slo*-type sub family (*Slo2.2*) of potassium channel genes, also known as Slack (sequence like a calcium activated potassium channel) and co-assembles with other *Slo* channel subunits[10–12]. *KCNT1* channels are highly expressed in many regions of the mammalian brain, including the frontal and piriform cortices[13]. While *KCNT1* channels are thought to play important roles in regulating neuronal excitability their precise function is yet to be resolved.

Mutations M896I, Y796H and R928C are substitutions of highly conserved residues in the intracellular C-terminal region adjacent to or within a putative nicotinamide adenine dinucleotide (NAD^+)-binding site, which has been proposed to modulate the sodium sensitivity of the channel[14]. The ADNFLE and EIMFS-associated mutations are located in the C-terminal region of the channel, near, or in close proximity to putative consensus sites for protein kinase C (PKC)[5–9]. Phosphorylation of the rodent *Kcnt1* by PMA, a PKC activator, has been shown to activate Slack currents expressed in *Xenopus* oocytes[15]. In their analysis of mutations associated with EIMFS, Barcia and colleagues[6] demonstrate a 'gain of function' and suggest this is due to mutant channels mimicking the effects of phosphorylation of the C-terminal domain by PKC.

The clinical severity of *KCNT1* gain-of-function disorders creates an urgent need for novel therapies. The FDA approved drug quinidine, in clinical use for treatment of cardiac arrhythmias for decades, reversibly blocks rodent *Kcnt1* channels[11,16]. As *KCNT1* disorders have such a severe prognosis, quinidine therapy may hold promise despite its known adverse effect profile.

The aims of the current study were to investigate the electrophysiological and pharmacological characteristics of ADNFLE-associated *KCNT1* mutations M896I, R398Q, Y796H, R928C, and compare them to those of the newly described EIMFS P924L mutation. We also sought to verify, using human clones, the earlier rodent *Kcnt1* functional reports of the EIMFS-associated mutations (R428Q and A934T)[6,8]. In addition, we assessed the effects of quinidine on human *KCNT1* WT and mutant channels. A further objective was to determine the neurodevelopmental time frame for the contribution of this channel to neuronal excitability by analysing the expression levels of m*Kcnt1* mRNA in mouse brain. A better understanding of these epilepsy mutations may provide us with a validated target for screening new drugs as well as assessing FDA approved drugs that may target *KCNT1* channels.

Materials and Methods

KCNT1 mutagenesis and *in vitro* transcription

Human h*KCNT1* (MIM 608167) and rat r*Kcnt1* coding sequences were synthesised by Genscript (Piscataway, NJ). The h*KCNT1* mutations c.2688G>A (M896I), c.1193G>A (R398Q), c.2386T>C (Y796H), c.2782C>T (R928C), c.1283G>A (R428Q), c.2800G>A (A934T), c.2771C>T (P924L) and the r*Kcnt1* mutant c.2719C>T/c.2721G>C (R907C) were generated by Genscript (Piscataway, NJ). The expression constructs were produced by inserting the wild-type (WT), mutated h*KCNT1* and r*Kcnt1* coding sequences into the pGEMHE vector[17] between restriction sites *Xba*I and *Eco*RI. Construct fidelity was confirmed by DNA sequencing. cDNAs were transcribed *in vitro* (mMessage mMachine, Ambion, Austin, TX).

Oocyte preparation

Xenopus oocytes (Dumont stage V or VI) were surgically removed from *Xenopus* laevis and were prepared as described previously[18]. Oocytes were kept in ND96 solution and stored at

17 °C. 50 nl of capped cRNA was injected into each oocyte using Roboinject1 System (Multi Channel Systems, Reutlingen, Germany). A total of 10 ng of cRNA was injected into each oocyte.

Electrophysiology recording

After 14–24 hr of expression, two electrode voltage clamp recording was performed using the Roboocyte2 System (Multi Channel Systems, Reutlingen, Germany). Oocytes were impaled with electrodes that contained 1.5 M K-acetate and 0.5 M KCl and were held at −90 mV and perfused with bath solution containing: (mM) 96 NaCl, 2 KCl, 1.8 $CaCl_2$, 1 $MgCl_2$, and 5 HEPES pH 7.5. Recording frequency was 1 kHz and temperature was maintained between 20–22 °C. To record expressed membrane currents from oocytes, the cells were held at −90 mV, and 600 ms duration test depolarisations were applied in 10 mV increments, from −80 mV to +80 mV, every 5 s. WT currents were always measured contemporaneously and with the same batch of oocytes with a mutant channel providing an internal control to address the possibility of batch-to-batch variation in expression. Phorbol 12-myristate 13-acetate (PMA) (Sigma-Aldrich, Castle Hill, NSW) was dissolved in DMSO (POCD Scientific, Gillman, SA) and applied by continuous perfusion for 1 min and incubated for a further 15 mins, followed by a 10 min washout. Quinidine (Sigma, St. Louis, MO) was dissolved in ethanol and applied by continuous perfusion for 1 min and incubated for a further 5 mins, followed by a 10 min washout. Currents were recorded before application of compound, in the presence of compound and following washout. Peak currents were measured at the end of each sweep for all clones, except for mutation R928C, where the peak currents were observed at the beginning of the sweep. The derived data is shown at +10 mV. At +10 mV currents from all of the mutated channels were usable, whereas, by stepping to potentials ≥+20 mV, current amplitudes in many cases were larger than the capacity of the amplifier. Current voltage relationship curves were produced using recordings that did not saturate the amplifier at +80 mV. Electrophysiological data were analysed using AxoGraph (AxoGraph Scientific, Sydney, Australia). Statistical analysis was performed on GraphPad Prism 6 (GraphPad Software, La Jolla, CA). Data are presented as mean ± S.E.M and Student's *t*-test was used to test statistical significance. One-way ANOVA with Bonferroni correction was applied to take into account multiple comparisons in Figure 1C.

Brain tissue collection and RNA extraction

Brains of male C57BL/6J mice were collected at seven postnatal ages (3 mice for each age group except hippocampus at P0 where 6 mice were used) and divided into 4 regions: cerebellum, thalamus, hippocampus and cortex. Tissue samples were frozen in liquid nitrogen and stored at −80 °C. Total RNA was extracted from the brain regions using Trizol reagent (Invitrogen) and RNeasy kit (Qiagen) following the manufacturer's instructions.

Quantitative RT-PCR

cDNAs were generated from 1 μg of total RNA using SuperScript III reverse transcriptase with random hexamer primers (Invitrogen). Quantitative PCR was performed using ViiA7 System (Applied Biosystems) and TaqMan Gene Expression Assays for mouse m*Kcnt1*, ubiquitin C (*Ubc*) and *g*lyceraldehyde 3-phosphate dehydrogenase (*Gapdh*) (Applied

Biosystems assay IDs Mm01330653_m1, Mm01198158_m1 and Mm99999915_g1, respectively). Relative quantities of m*Kcnt1* mRNA were calculated using qbase+ software (http://www.biogazelle.com/qbaseplus[19].) *Ubc* and *Gapdh* were used as normalisation factors[20,21]. Relative quantities of the m*Kcnt1*, *Ubc* and *Gapdh* mRNAs in the cerebellum at P0 were arbitrarily defined as 1.

Results

Gain-of-function channel phenotype with *KCNT1* mutations

The electrophysiological properties of human *KCNT1* mutations, identified in patients with ADNFLE[5] (M896I, R398Q, Y796H and R928C) and in patients with EIMFS[6,8,9] (R428Q, A934T and P924L), were analysed in *Xenopus* oocytes. WT and mutant channels produced voltage activated currents and, as expected, water injection controls did not differ from uninjected oocytes with only small contributions of endogenous currents (Fig 1A). Representative current family traces from WT and mutant channels contrasting current amplitudes, kinetics and voltage dependencies are shown (Fig 1A). Visual inspection of raw current traces showed a clear trend that disease causing mutations increase current magnitude and in some cases hasten (M896I, R928C and A934T) or slow (R398Q) activation.

Quantification of current amplitude was measured at a potential of +10 mV to avoid biasing averages caused by censoring data that saturated the amplifier at higher depolarising potentials. Without exception, the mutated channels yielded larger currents (Fig 1A and 1B), providing the first view into the mechanism of pathogenicity for ADNFLE[5] and revealing the functional deficit of the recently ascertained EIMFS case[9]. Furthermore, our analysis verified earlier functional data on the reported EIMFS mutants[6] (R428Q and A934T) that used a rodent *Kcnt1* assay. Our results show that, across independent studies, ‘gain of function’ is a common pathogenic feature of h*KCNT1* disorders. Pooling of currents across mutations associated with ADNFLE and comparison with the pooled average of the mutations associated with EIMFS, revealed a significant difference between the two groups (Fig 1C). While mutations from ADNFLE cases were associated with currents that were approximately 3 fold larger than WT, the mutations associated with the more severe syndrome of EIMFS were on average around 5 fold greater. To examine the possible effects that the different mutations might confer on the activation kinetics of channel currents, time to peak current was measured at +10 mV. M896I, R928C and A934T activate significantly faster, while R398Q, Y796H and P924L activate significantly slower than WT ($p<0.05$; Fig 1D). In addition, tail currents associated with channel closing were examined to determine the possible effects of the different mutations on deactivation kinetics. The tail currents for M896I, R928C, R428Q and P924L decay significantly slower than WT ($p<0.05$; Fig 1E), however, no significant differences were observed for R398Q, Y796H or A934T. These data suggest that the mutations not only cause an increase in current amplitude, but also modulate channel activation and deactivation kinetics. However, there was no apparent association of activation or deactivation kinetics with disease severity.

Current-voltage (*I/V*) curves, normalised to maximum current and averaged, were calculated for WT and mutant channels. As expected for *KCNT1*[10], they show mild voltage-

dependence of activation (Fig 1F and 1G). The shape of *I/V* curves for WT and some of the mutants did not vary, however, the *I/V* for M896I, R928C, A934T and P924L display a curious rollover of the curve at more depolarised potentials suggestive of saturation of conduction paths or appearance of a high voltage inactivation state.

Pharmacological modulation

To explore the therapeutic potential of quinidine we first determined whether it inhibits h*KCNT1* channels similarly to the rodent channels and then assessed the impact on mutant h*KCNT1*. Quinidine significantly inhibited WT h*KCNT1* at both 100 and 300 μM (Fig 2A and C), whereas its vehicle, ethanol, was without effect (data not shown). Representative current traces after application of 300 μM quinidine illustrate a clear block of current amplitude, which was reversible upon washout (Fig 2A). We next investigated the action of quinidine on mutant h*KCNT1* channels. Representative current traces from the h*KCNT1* R928C mutant channel after application of 300 μM quinidine illustrate a clear block of current amplitude, which was again reversible upon washout (Fig 2B). Furthermore, *I/V* curves for R928C in the presence of quinidine 300 μM were similar to the shape of the WT *I/V* curves (Fig 2C). A summary of the relative blocking effect of quinidine showed that for all of the mutant channels, 300 μM quinidine produced a significant block (Fig 2D), which was reversible upon washout. In some cases this block brought current levels down towards WT control values. It was apparent that some mutant channels were more sensitive to quinidine than others.

To examine whether quinidine alters channel kinetics, time to peak current and the tail current decay time was measured before and after application of quinidine (300 μM) at +10 mV (Fig 2E and F). At +10 mV the time to peak current for M896I was significantly slower than vehicle control. For mutants R428Q and P924L the time to peak current was significantly faster than vehicle control. For the other mutations (R398Q, Y796H, R928C and A934T), no significant differences were observed. Furthermore, quinidine did not affect the tail current decay time for the WT or the mutant channels. Quinidine reverses many of the changes in *I/V* curves in the mutant channels presumably as a consequence of altering voltage sensitivity.

Rodent *Kcnt1* currents are thought to be activated by $G\alpha_q$-protein coupled receptor stimulation via PKC[15]. As this modulatory effect has not been demonstrated with human *KCNT1*, we performed experiments using the PKC activator PMA to establish whether human channels expressed in oocytes are also sensitive to phosphorylation by PKC. Control currents were generated in the presence of vehicle and then again following 15 mins incubation with PMA (100 nM). In stark contrast to earlier work on the rodent *Kcnt1* currents, we observed significant inhibition of current by PMA for human WT and all human mutant channels ($p<0.0001$; Fig 3A). Furthermore, this inhibition was not reversible upon washout and no effect of the vehicle, DMSO, was observed (data not shown). These data suggest that phosphorylation of the h*KCNT1* channels by PKC has an inhibitory effect, much like that seen with the *Slo*2.1 channel, but in contrast to that observed in *Slo*2.2 channels[15]. To exclude a possible species difference, we expressed the rat WT r*Kcnt1* channel, as well as the mutant R907C which aligns with the mutant R928C h*KCNT1*

channel. Representative current family traces illustrate the different current amplitudes (Fig 3B). Application of PMA (100 nM) produced a small, but significant, inhibition of the WT r*Kcnt1* channel currents. However, it had no effect on the mutant R907C r*Kcnt1* channel currents (Fig 3C). We did, however, observe a significant increase in current amplitude for R907C when compared to WT r*Kcnt1* channels.

Regional and temporal expression of m*Kcnt1* mRNA in the developing mouse brain

In a final series of experiments we quantified the relative levels of mouse *Kcnt1* mRNA expression in the thalamus, hippocampus, cortex and cerebellum from postnatal day 0 through to 39 using quantitative RT-PCR (Fig 4). At birth, m*Kcnt1* mRNA was expressed at similar levels throughout the brain. In hippocampus and thalamus this expression level essentially remained unchanged over the course of postnatal development. In contrast, cortical m*Kcnt1* expression increased 3-fold during the first two weeks of life, remaining constant thereafter. A similar overall increase in expression occurred in the cerebellum, however, the onset was delayed until P9.

Discussion

In this study we present functional and pharmacological data, characterising *KCNT1* mutations associated with ADNFLE and EIMFS. We demonstrate that all pathogenic mutations result in channels which display a strong gain-of-function phenotype. This observation is of interest given recent population genetic analyses showing strong selection against functional variation in *KCNT1*[22]. In light of these findings, it is of particular interest that all the mutations identified to date are associated with a striking gain-of-function phenotype *in vitro*. Moreover the magnitude of this gain-of-function in the EIMFS group was greater than that associated with the less severe ADNFLE phenotype. While there may be other factors that contribute to the finer grained aspect of phenotype, such as genetic background, collectively, these data suggest that the *KCNT1* gain-of-function phenotype is directly pathogenic, and that amelioration or elimination of this gain-of-function may be an effective treatment in patients with *KCNT1* disorders. The demonstration here that quinidine can reverse the mutation specific gain-of-function provides clear indication that these conditions may respond to targeted therapy.

Previous studies have suggested that rodent *Kcnt1* channel activation is potentiated through phosphorylation involving PKC[15] and EIMFS mutations are postulated to be in a constitutive PKC phosphorylated-like state[6]. Our data show that the PKC activator, PMA, causes a significant reduction in current for all human mutant channels tested. The basis of the discrepancy between our data and that previously published is unclear. One possibility explored is the potential confound of species difference. A lack of effect of PMA on the mutant rat R907C channel is consistent with that published by Barcia and colleagues (2012). Although the sensitivity of human and rodent WT channels to PMA was different, in both cases it causes a reduction in current which is in contrast with that observed previously[6,15]. Therefore, a phosphorylation-like state of the channel does not seem a likely explanation for the gain-of-function mechanism seen with these mutations.

The mechanisms underlying increased neuronal excitability, due to a gain-of-function of the *KCNT1* channels are not known. Large elevations in intracellular sodium concentrations, which occur during normal physiological signalling in the nervous system, are sensed by sodium activated potassium channels, such as *KCNT1*. These channels are particularly highly expressed in neurons[13] and are able to influence neuronal firing patterns, either through rapid activation with a single action potential that could increase firing rates, or slow activation during repetitive firing that could decrease firing rates[23]. The clear association of *KCNT1* gain-of-function and disease severity suggests that either or both of these mechanisms are at play to increase network excitability in ADNFLE and EIMFS. In excitatory neurons, the higher currents generated by the mutant *KCNT1* channels may enable shortening of action potential (AP) by permitting a more rapid repolarisation in response to increased sodium concentrations during the AP upstroke. Therefore, increases in repolarisation rates could be the mechanism that enables higher action potential firing rates in *KCNT1* based epilepsies. Experimental evidence for this idea is provided by studies of the electrocytes of the electric fish, *Gymnotus carapo*[24,25], where *KCNT1* channels are highly expressed and thought to be critical for enabling firing rates of up to 500 Hz. *KCNT1* channels are also expressed in interneurons[13] raising the possibility that disinhibition may also play a role in disease pathology. Sustained firing of fast spiking interneurons may result in accumulation of intracellular Na^+ sufficient to slowly activate *KCNT1* channels to produce a long lived hyperpolarisation. In the case of mutant *KCNT1* channels, with enhanced currents, this hyperpolarisation would be greater and would result in more disinhibition than would occur in neurons with WT channels. *KCNT1* mutations may be altering the channels sensitivity to sodium in a similar way to that observed with a mutation in the large conductance calcium-sensitive potassium channel (BK) which has been associated with a human syndrome of coexistent generalised epilepsy and paroxysmal dyskinesia (GEPD)[26]. This mutation in the α subunit of the BK channel, which has enhanced macroscopic currents, was reported to cause GEPD as a result of an increased channel opening probability and increased calcium sensitivity. Moreover, the mutation has subsequently been shown to mediate the allosteric coupling between calcium binding and channel opening[27]. If *KCNT1* mutations are increasing the channels sensitivity to cytosolic sodium concentrations, this could indeed account for increased excitability by inducing rapid repolarization of the action potential, allowing neurons to fire at a more rapid rate. The precise contribution to network pathology of ADNFLE and EIMFS cannot be fully determined until animal models are available to study the molecular and temporal contexts in which rapid and slow modulation of neuronal firing by *KCNT1* channels can be dissected.

ADNFLE and EIMFS are strikingly different epilepsy syndromes. The discovery that they were allelic was completely unexpected and seemingly paradoxical. The physiological and expression data observations reported here may explain this. EIMFS begins in early infancy, while ADNFLE begins much later in mid-childhood; this difference in age of onset may be due to differences in the level of gain-of-function produced by the mutations. A 5 fold gain-of-function is an extreme modification, which most likely accounts for the earlier onset of symptoms and pathological network excitability in the immature infant brain resulting in the chaotic, refractory, ongoing multifocal seizures of EIMFS. The 3 fold change observed with ADNFLE mutants may not be sufficient to cause seizures until later in development, when

greater expression of *KCNT1* is likely and brain excitability is sufficiently elevated. By this age, the more mature brain may alter the impact of the *KCNT1* gain-of-function potentially limiting pathology to frontal networks with the phenotype manifesting as nocturnal frontal lobe epilepsy.

The hallmark of ADNFLE is nocturnal frontal lobe seizures. The expression of *KCNT1* in the frontal cortex[13] and its greater expression in the mouse cortex, shown here, ideally positions *KCNT1* to contribute to frontal lobe seizures. Regarding the nocturnal occurrence of ADNFLE, Tamsett and colleagues[14] demonstrated that NAD^+ and $NADP^+$ activate Slack channels expressed in HEK293 cells, as well as neuronal sodium-activated potassium channels. M896I, Y796H and R928C are substitutions of highly conserved residues in the intracellular cytoplasmic terminal region adjacent to or within a putative NAD^+-binding site, which has been proposed to modulate the sodium sensitivity of the channel. The circadian clock synchronizes behaviour and metabolism with the light-dark cycle and levels of NAD^+ display circadian oscillations, which are regulated by the core clock machinery in mice[28]. This is particularly interesting as *KCNT1* channels are modulated by NAD^+ and also associated with nocturnal epilepsy[5], but it is yet to be determined whether the mutated proteins have an altered sensitivity to NAD^+ or $NADP^+$. To investigate this more fully a mammalian expression system, where intracellular modulators such as NAD^+ can be more easily manipulated, would provide more detailed high fidelity biophysical data. However, we encountered significant challenges with poor expression levels and cell death when attempting to extend our investigation in HEK293 cells, rendering them a poor model for assessing gain-of-function of mutant *KCNT1* channels.

Although the mechanism of the gain-of-function is not fully understood, it is known that quinidine can block rodent *Kcnt1* channels[11,16]. In agreement with this, we have demonstrated that quinidine produces a reversible block of all human WT and mutant h*KCNT1* channels studied here. The mutations have different sensitivities to quinidine, but all can be blocked regardless of their associated clinical phenotype. Another antiarrhythmic compound, clofilium, also inhibits Slack channels expressed in *Xenopus* oocytes[29]. In the absence of specific blockers for this channel, quinidine, which penetrates the blood brain barrier (BBB)[30] and clofilium, with its large hydrophobic alkyl side chains suggesting it should cross the BBB[31], may be potential oral therapeutic agents for ADNFLE and EIMFS patients carrying a mutated *KCNT1* gene. Future clinical studies could establish a potential therapeutic effect and dosing regimens. Furthermore, greater insights into the mechanisms of action of these mutations may provide us with a validated target for developing quinidine analogues with improved efficacy and safety profiles or even novel chemical classes.

Acknowledgments

We thank the families for their participation in this study. This work was supported by the Victorian Government through the Operational Infrastructure Scheme. This work was supported by the following grants from the National Health and Medical Research Council of Australia: program grant: (Program Grant 628952 to S.F.B., I.E.S., S.P. and L.M.D., Training Fellowship 1016715 to S.E.H., Senior Research Fellowship 1005050 to S.P., Australia Fellowship 466671 to S.F.B., Practitioner Fellowship 1006110 to I.E.S. and Career Development Fellowship 1032603 to L.M.D.). We thank Dr Daniel Lowenstein and colleagues from the Epilepsy Phenome/Genome Project (epgp.org; supported by grant NS053998 from the National Institute of Neurological Disorders and Stroke - NINDS) and Epi4K (epi4K.org; supported by grants NS053998, NS077274, NS077303 and NS077276 from NINDS) for their collaborative efforts that led to the identification of the individual with the P924L mutation

included in this study. All experiments were performed in accordance with relevant animal ethical guidelines and approvals.

References

1. Derry CP, Heron SE, Phillips F, et al. Severe autosomal dominant nocturnal frontal lobe epilepsy associated with psychiatric disorders and intellectual disability. Epilepsia. 2008; 49:2125–2129. [PubMed: 18479385]
2. Coppola PP, Chirin C, Robain O, Dulac O. Migrating partial seizures in infancy: a malignant disorder with developmental arrest. Epilepsia. 1995; 36:1017–1024. [PubMed: 7555952]
3. Berg AT, Berkovic SF, Brodie MJ, et al. Revised terminology and concepts for organization of seizures and epilepsies: report of the ILAE Commission on Classification and Terminology, 2005–2009. Epilepsia. 2010; 51:676–685. [PubMed: 20196795]
4. Steinlein, OK.; Kaneko, S.; Hirose, S. Jasper's basic mechanisms of the epilepsies [Internet]. 4th ed.. Bethesda: 2012. Nicotinic acetylcholine receptor mutations.
5. Heron SE, Smith KR, Bahlo M, et al. Missense mutations in the sodium-gated potassium channel gene *KCNT1* cause severe autosomal dominant nocturnal frontal lobe epilepsy. Nat Genet. 2012; 44:1188–1190. [PubMed: 23086396]
6. Barcia G, Fleming MR, Deligniere A, et al. *De novo* gain-of-function *KCNT1* channel mutations cause malignant migrating partial seizures of infancy. Nat Genet. 2012; 44:1255–1260. [PubMed: 23086397]
7. Ishii A, Shioda M, Okumura A, et al. A recurrent *KCNT1* mutation in two sporadic cases with malignant migrating partial seizures in infancy. Gene. 2013; 531:467–471. [PubMed: 24029078]
8. McTague A, Appleton R, Avula S, et al. Migrating partial seizures of infancy: expansion of the electroclinical, radiological and pathological disease spectrum. Brain. 2013; 136:1578–1591. [PubMed: 23599387]
9. Epi4K Consortium & Epilepsy Phenome/Genome Project. *De novo* mutations in epileptic encephalopathies. Nature. 2013; 501:217–221. [PubMed: 23934111]
10. Joiner WJ, Tang MD, Wang L-Y, et al. Formation of intermediate-conductance calcium-activated potassium channels by interaction of Slack and Slo subunits. Nat Neurosci. 1998; 1:462–469. [PubMed: 10196543]
11. Bhattacharjee A, Joiner WJ, Wu M, et al. Slick (Slo2.1), a Rapidly-gating sodium-activated potassium channel inhibited by ATP. J Neurosci. 2003; 23:11681–11691. [PubMed: 14684870]
12. Yuan A, Santi CM, Wei A, et al. The sodium-activated potassium channel is encoded by a member of the *Slo* gene family. Neuron. 2003; 37:765–773. [PubMed: 12628167]
13. Bhattacharjee A, Gan L, Kaczmarek LK. Localization of the Slack potassium channel in the rat central nervous system. J Comp Neurol. 2002; 454:241–254. [PubMed: 12442315]
14. Tamsett TJ, Picchione KE, Bhattacharjee A. NAD^+ activates K_{Na} channels in dorsal root ganglion neurons. J Neurosci. 2009; 29:5127–5134. [PubMed: 19386908]
15. Santi CM, Ferreira G, Yang B, et al. Opposite regulation of Slick and Slack K channels by neuromodulators. J Neurosci. 2006; 26:5059–5068. [PubMed: 16687497]
16. Yang B, Gribkoff VK, Pan J, et al. Pharmacological activation and inhibition of *Slack* (*Slo*2.2) channels. Neuropharm. 2006; 51:896–906.
17. Lima ER, Tytgat J, Hess P. Subunit stoichiometry of a mammalian K^+ channel determined by construction of multimeric cDNAs. Neuron. 1992; 9:861–871. [PubMed: 1419000]
18. Petrou S, Ugur M, Drummond RM, et al. P2X7 purinoceptor expression in *Xenopus* oocytes is not sufficient to produce a pore-forming P2Z-like phenotype. FEBS Lett. 1997; 411:339–345. [PubMed: 9271232]
19. Hellemans J, Mortier G, De Paepe A, et al. qBase relative quantification framework and software for management and automated analysis of real-time quantitative PCR data. Genome Biology. 2007; 8:R19.1–R19.14. [PubMed: 17291332]
20. Vandesompele J, De Preter K, Pattyn F, et al. Accurate normalization of real-time quantitative RT-PCR data by geometric averaging of multiple internal control genes. Genome Biology. 2002; 3 Research/0034.

21. Candenas L, Seda M, Noheda P, et al. Molecular diversity of voltage-gated sodium channel α and β subunit mRNAs in human tissues. Eur J Pharmacol. 2006; 541:9–16. [PubMed: 16750188]
22. Petrovski S, Wang Q, Heinzen EL, et al. Genic intolerance to functional variation and the interpretation of personal genomes. PLoS Genet. 2013; 9:1–13.
23. Bhattacharjee A, Kaczmarek LK. For K^+ channels, Na^+ is the new Ca^{2+} Trends Neurosci. 2005; 28:422–428. [PubMed: 15979166]
24. Sierra F, Comas V, Buno W, Macadar O. Sodium-dependent plateau potentials in electrocytes of the electric fish *Gymnotus carapo*. J Comp Physiol. 2005; 191:1–11. [PubMed: 15372305]
25. Markham M, Kaczmarek LK, Zakon HH. A sodium-activated potassium channel supports high-frequency firing and reduces energetic costs during rapid modulations of action potential amplitude. J Neurophysiol. 2013; 109:1713–1723. [PubMed: 23324315]
26. Du W, Bautista JF, Yang H, et al. Calcium-sensitive potassium channelopathy in human epilepsy and paroxysmal movement disorder. Nat Genet. 2005; 37:733–738. [PubMed: 15937479]
27. Yang J, Krishnamoorthy G, Saxena A, et al. An epilepsy/dyskinesia-associated mutation enhances BK channel activation by potentiating Ca^{2+} sensing. Neuron. 2010; 66:871–883. [PubMed: 20620873]
28. Ramsey KM, Yoshino J, Brace CS, et al. Circadian clock feedback cycle through NAMPT-mediated NAD^+ biosynthesis. Science. 2009; 324:651–654. [PubMed: 19299583]
29. de Los Angeles Tejada M, Stolpe K, Meinild A-K, Klaerke DA. Clofilium inhibits Slick and Slack potassium channels. Biologics. 2012; 6:465–470. [PubMed: 23271893]
30. Harashima H, Sawada Y, Sugiyama Y, et al. Analysis of nonlinear tissue distribution of quinidine in rats by physiologically based pharmacokinetics. J Pharmacokinet Biopharm. 1985; 13:425–440. [PubMed: 4087170]
31. Castle NA. Selective inhibition of potassium currents in rat ventricle by clofilium and its tertiary homolog. J Pharmacol Exp Ther. 1991; 257:342–350. [PubMed: 2019997]

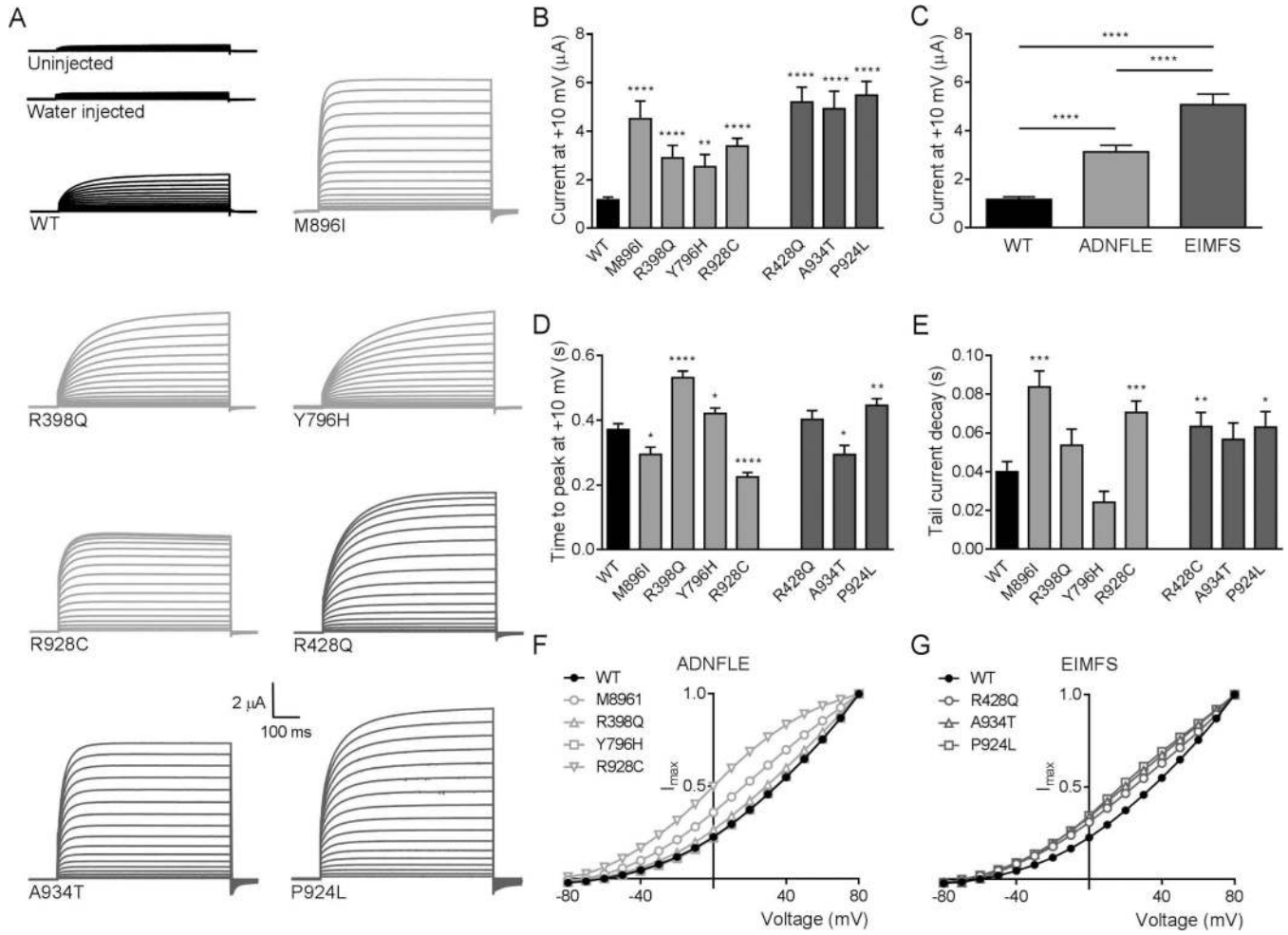

Figure 1.

h*KCNT1* wild-type and mutant currents recorded in *Xenopus* oocytes. (A) Representative current traces obtained from uninjected and water injected oocytes and oocytes expressing wild-type (▬ WT), ADNFLE (▬ M896I, R398Q, Y796H, R928C) and EIMFS (▬ R428Q, A934T and P924L) channels. Oocytes were held at −90 mV and stepped from −80 mV to 80 mV for 600 ms every 5 s. Scale bars apply to all traces. (B) Average peak currents at +10 mV for WT (n=127), M896I (n=39), R398Q (n=41), Y796H (n=63), R928C (n=51), R428Q (n=38), A934T (n=38) and P924L (n=64) channels. The peak currents for each mutant channel at +10 mV were compared to the peak currents for the WT channel at +10 mV. (C) Comparison of pooled currents at +10 mV. WT (■, n=127) and pooled ADNFLE (■, n=194) and pooled EIMFS (■, n=140). (D) Activation kinetics shown as mean time to peak current at +10 mV for WT, M896I, R398Q, Y796H, R928C, R428Q, A934T and P924L channels (see B for n values). The time to peak current for each mutant channel at +10 mV was compared to the time to peak current for the WT channel at +10 mV. (E) Average tail current decay time at +10 mV for WT (n=62), M896I (n=15), R398Q (n=27), Y796H (n=35), R928C (n=40), R428Q (n=36), A934T (n=28) and P924L (n=28) channels. Decay time for each mutant channel was compared to WT. WT (■), ADNFLE (■) and EIMFS (■). (F) Averaged and normalised current-voltage relationships for WT (●, n=127), M896I (○,

n=32), R398Q (△, n=37), Y796H (□, n=51), R928C (▽, n=46). (G) Averaged and normalised current-voltage relationships for WT (●, n=127), R428Q (○, n=32), A934T (△, n=34) and P924L (□, n=29) channels. Currents were normalized to the value at a test potential of +80 mV (I_{max}). (*p< 0.05; **p< 0.01; *** p< 0.001; ****p<0.0001).

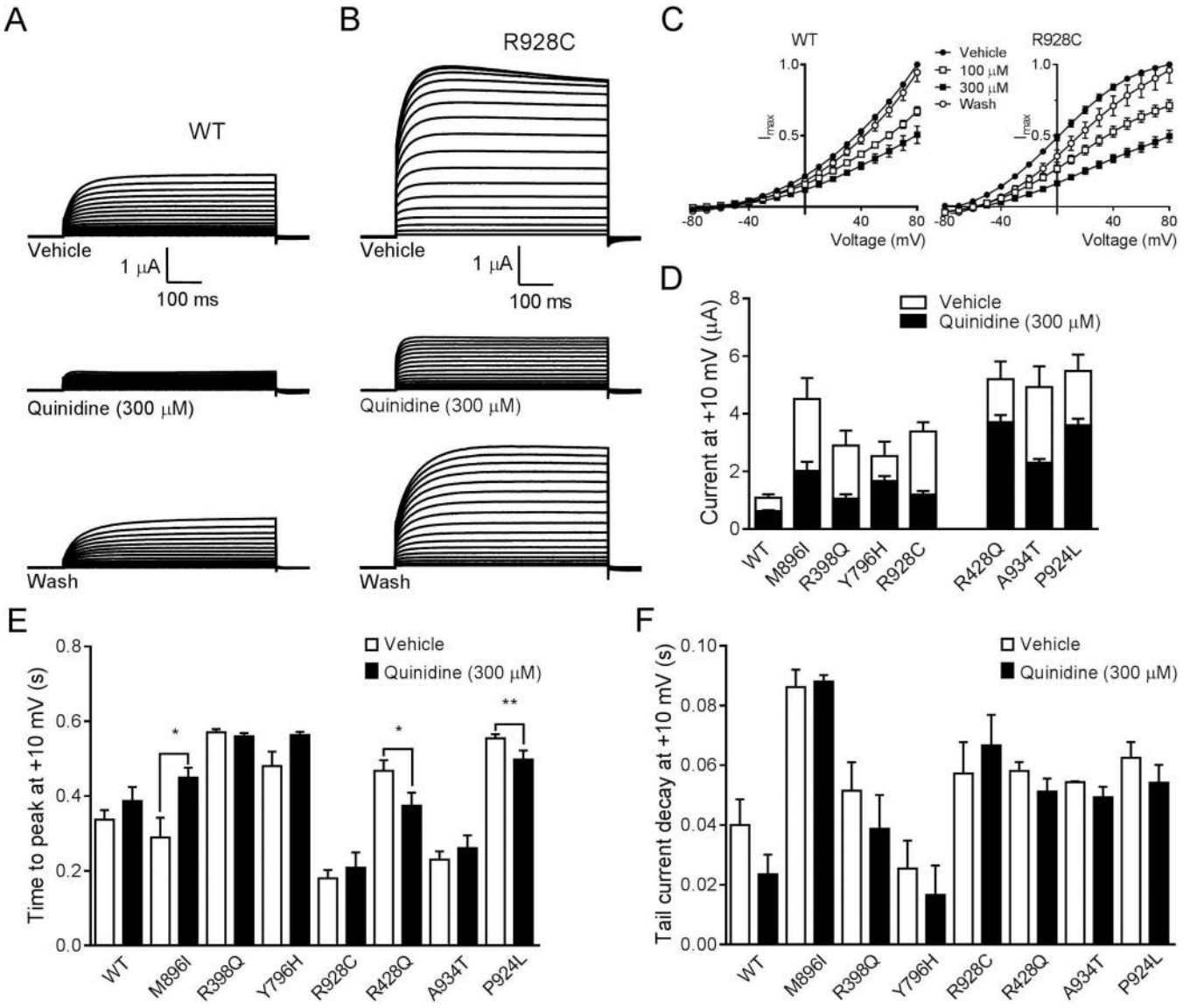

Figure 2.

Quinidine inhibition of h*KCNT1* currents expressed in *Xenopus* oocytes. (A) Current traces from WT in vehicle control, in the presence of 300 μM quinidine and following washout of quinidine. Scale bars apply to all traces. (B) Current recordings from R928C mutant in vehicle control, in the presence of 300 μM quinidine and following washout of quinidine. Scale bars apply to all traces. (C) Normalised average current-voltage relationships for WT and mutant R928C in the presence of vehicle (●; WT n=50, R928C n=26), 100 μM (□; WT n=30, R928C n=12) and 300 μM quinidine (■; WT n=20, R928C n=14) followed by washout of 300 μM quinidine (○; WT n=20, R928C n=14). Currents were normalized to the value in the absence of quinidine at a test potential of +80 mV (I_{max}). (D) Comparison of average current amplitude for WT and mutant channels illustrating the degree of block by 300 μM quinidine (WT n=13; M896I n=5; R398Q n=8; Y796H n=9; R928C n=14; R428Q n=24; A934T n=15 and P924L n=34) derived from measurements made at +10 mV (see Fig 1B for vehicle control n values). (E) Average time to reach peak current amplitude for WT

(n=13), M896I (n=5), R398Q (n=8), Y796H (n=9), R928C (n=14), R428Q (n=24), A934T (n=15) and P924L (n=34) mutant channels at +10 mV before and after application of quinidine (300 μM). (*p< 0.05;**p< 0.01). (F) Average tail current decay time at +10 mV for WT (n=13), M896I (n=5), R398Q (n=8), Y796H (n=9), R928C (n=14), R428Q (n=24), A934T (n=15) and P924L (n=34) mutant channels before and after application of quinidine (300 μM).

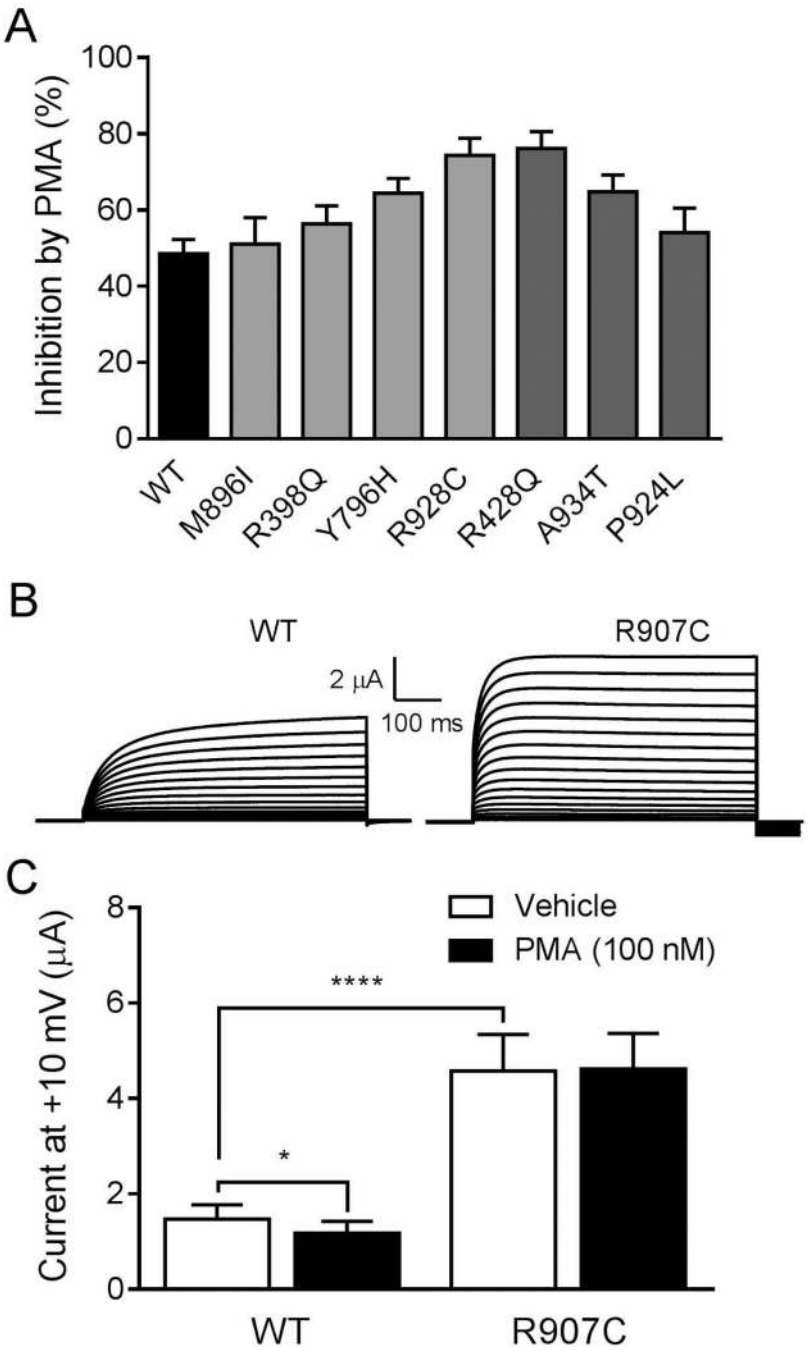

Figure 3.

PMA inhibition of h*KCNT1* and r*Kcnt1* currents expressed in *Xenopus* oocytes. (A) Average percent inhibition at +10 mV of WT (n=58), M896I (n=18), R398Q (n=25), Y796H (n=47), R928C (n=34), R428Q (n=9), A934T (n=25) and P924L (n=17) h*KCNT1* channels by PMA (100 nM). WT (■), ADNFLE (■) and EIMFS (■). (B) Representative current traces obtained from oocytes expressing WT and mutant R907C r*Kcnt1* channels. Scale bars apply to all traces. (C) Average peak currents at +10 mV for WT (n=51) and R907C (n=37) r*Kcnt1* channels in the presence of vehicle and then following application of PMA (100 nM). The

peak currents for WT and R907C r*Kcnt1* in the presence of vehicle were compared to each other and to the peak currents in the presence of PMA (100 nM). (*$p < 0.05$;***$p < 0.001$).

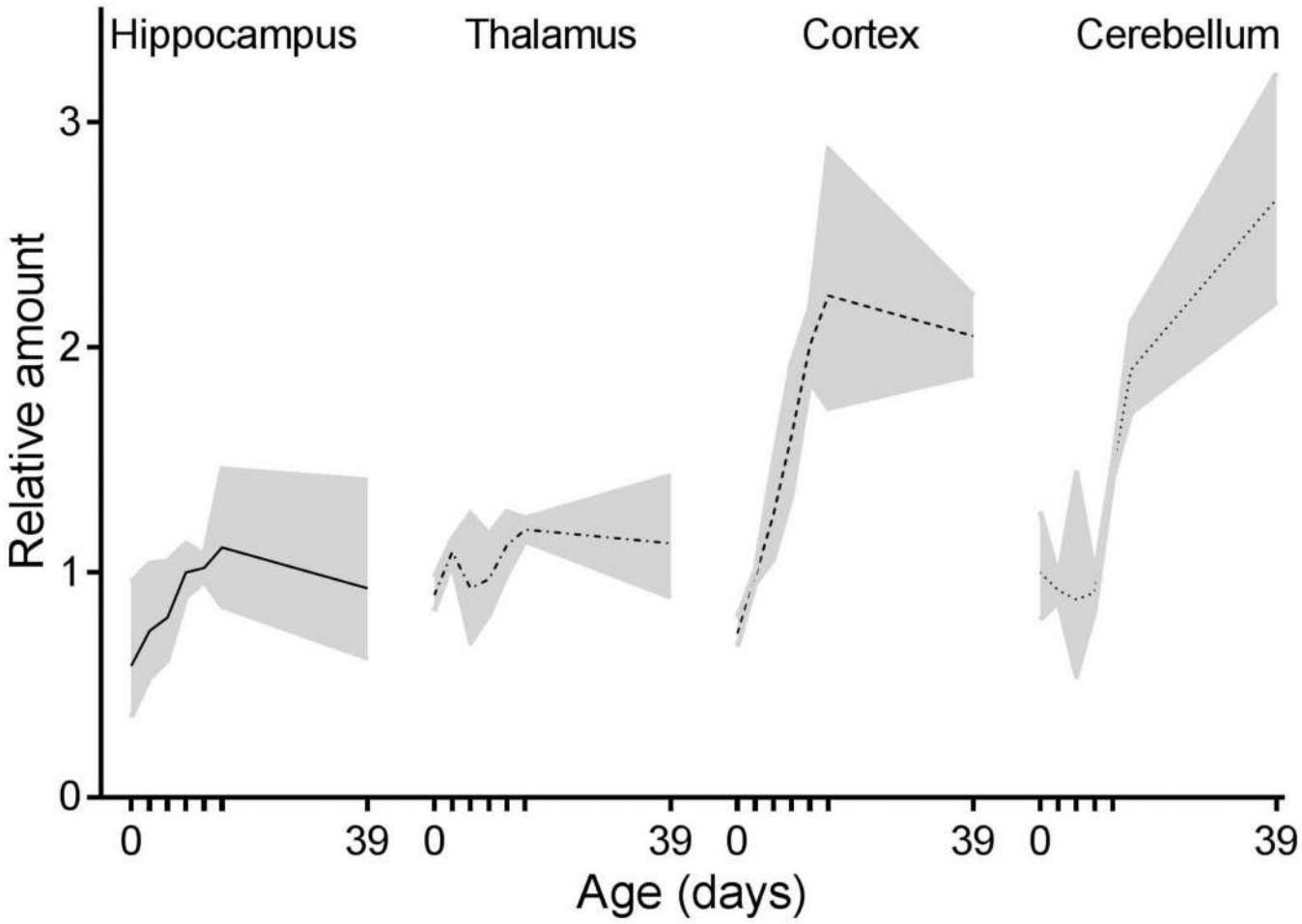

Figure 4.

Quantitative RT-PCR analysis of m*Kcnt1* mRNA expression in developing mouse brain. Samples were taken at seven postnatal ages (0, 3, 6, 9, 12, 15 and 39 days). Hippocampus (solid line), thalamus (dot-dash line), cortex (dashed line) and cerebellum (dotted line). Relative amount of m*Kcnt1* mRNA in cerebellum at day 0 was defined as one. The data points are averages of samples from at least three mice, with 95 % confidence interval shown as shaded filled area.